Quantifying Rainfall in Greenland: A Combined Observational and Modeling Approach

BAOJUAN HUAI,[a] MICHIEL R. VAN DEN BROEKE,[b] CARLEEN H. REIJMER,[b] AND JOHN CAPPELLEN[c]

[a] *College of Geography and Environment, Shandong Normal University, Jinan, China*
[b] *Institute for Marine and Atmospheric Research, Utrecht University, Utrecht, Netherlands*
[c] *Danish Meteorological Institute, Copenhagen, Denmark*

(Manuscript received 14 December 2020, in final form 16 June 2021)

ABSTRACT: This paper estimates rainfall totals at 17 Greenland meteorological stations, subjecting data from in situ precipitation gauge measurements to seven different precipitation phase schemes to separate rainfall and snowfall amounts. To correct the resulting snow/rain fractions for undercatch, we subsequently use a dynamic correction model (DCM) for automatic weather stations (AWS, Pluvio gauges) and a regression analysis correction method for staffed stations (Hellmann gauges). With observations ranging from 5% to 57% for cumulative totals, rainfall accounts for a considerable fraction of total annual precipitation over Greenland's coastal regions, with the highest rain fraction in the south (Narsarsuaq). Monthly precipitation and rainfall totals are used to evaluate the regional climate model RACMO2.3. The model realistically captures monthly rainfall and total precipitation (R = 0.3–0.9), with generally higher correlations for rainfall for which the undercatch correction factors (1.02–1.40) are smaller than those for snowfall (1.27–2.80), and hence the observations are more robust. With a horizontal resolution of 5.5 km and simulation period from 1958 to the present, RACMO2.3 therefore is a useful tool to study spatial and temporal variability of rainfall in Greenland, although further statistical downscaling may be required to resolve the steep rainfall gradients.

KEYWORDS: Precipitation; Rainfall; Automatic weather stations; Data quality control; Gauges; Regional models

1. Introduction

Precipitation (snowfall plus rainfall) determines the hydrology of the Greenland tundra, but it also is the main positive contributor to the mass balance of the Greenland ice sheet (GrIS; Box et al. 2006; Van den Broeke et al. 2009). Not only the total precipitation amount, but also the precipitation phase (liquid or solid) plays an important role in the mass balance, surface energy balance (Noël et al. 2015), hydrology, and dynamics of the GrIS. Rain that falls on impenetrable bare ice usually runs off quickly (Smith et al. 2015), either supra- or englacially, but rain that falls on snow will be partly retained by capillary forces and/or refreezing. Recently, Doyle et al. (2015) reported widespread ice flow acceleration that extended 140 km into the GrIS interior, following extreme surface runoff from melt and rainfall. Rainfall is also important for the dynamics of the seasonal snow cover in the ice-free part of Greenland, where it can, for example, release avalanches as a result of snow wetting (Abermann et al. 2019).

A future decline in snowfall over the GrIS is diagnosed as being almost entirely caused by changes in precipitation phase (snow turning into rain) with little change in total precipitation (Screen and Simmonds 2012). More rainfall on the ice sheet directly leads to more runoff (Colgan et al. 2011) compared with snow, which first accumulates before it melts and runs off as meltwater. As rainfall over Greenland is expected to become more widespread and frequent in a further warming atmosphere, it represents a relatively poorly known vulnerability of the GrIS to climate change (Doyle et al. 2015). A comprehensive understanding of precipitation rate and phase in Greenland is therefore not only relevant to understand the current, but also the future mass balance of the GrIS.

Numerous studies have used a variety of methods to infer precipitation rate and phase over Greenland, often based on extrapolation of observations and/or model simulations (Ohmura and Reeh 1991; Chen et al. 1997; Yang et al. 1999; Bales et al. 2009; Box et al. 2006). In spite of these efforts, comparison studies show 25%–40% or even larger differences in total precipitation estimates over the GrIS between different models (Cullather et al. 2014; Fettweis et al. 2020). A reasonably robust model evaluation can be made for total accumulation in the interior ice sheet (above the percolation zone) using snow accumulation estimates from ice cores, snow pits, and snow radar (Lewis et al. 2019). Automatic weather stations of the Greenland Climate Network situated mainly in the accumulation zone (GC-NET; Steffen and Box 2001) infer snow accumulation event size from surface height measurements using sonic rangers. In the ablation zone of the GrIS, automatic weather stations (AWS) of the Programme for Monitoring of the Greenland Ice Sheet (PROMICE) do the same, and some are even equipped with rain gauges (Van As et al. 2017).

Along the ice-free periphery of Greenland, multiple meteorological stations have been and/or are still operated by the Danish Meteorological Institute (DMI) since 1958 (Cappelen 2020), measuring precipitation using a variety of rain gauges.

Denotes content that is immediately available upon publication as open access.

Supplemental information related to this paper is available at the Journals Online website: https://doi.org/10.1175/JAMC-D-20-0284.s1.

Corresponding author: Baojuan Huai, huaibaojuan@126.com

DOI: 10.1175/JAMC-D-20-0284.1

Precipitation gauge measurements have several well-known error sources, such as wind-induced undercatch due to wind field deformation, wetting loss, and evaporation losses, which especially impact solid precipitation measurement accuracy (Yang et al. 1999). These systematic errors, which mostly lead to an underestimation of actual precipitation (Yang et al. 1995; Walsh et al. 1998; Yang et al. 1998) vary by phase of precipitation (rain, mixed, snow) and gauge types. The systematic error of solid precipitation is commonly greater than the error for liquid precipitation (WMO 2008). In particular, gauge measurements of snowfall, which in Greenland are primarily confined to the topographically complex coastal regions, are strongly contaminated by wind effects (Metcalfe et al. 1994; Bromwich et al. 1998; Yang et al. 1999).

Especially for places like Greenland, it is vital that these errors are corrected prior to their use in quantitative applications such as model evaluation (Michelson 2004). In 1986, the World Meteorological Organization (WMO) confirmed the need to make a special effort to improve the quality of point measurements of precipitation (Goodison et al. 1998). Yang et al. (1999) used a statistical method to bias correct daily Hellmann gauge precipitation measurements for wind-induced undercatch, wetting loss, and trace amount of precipitation at 12 meteorological stations in Greenland. Mernild et al. (2015) use a mean bias correction multiplier for precipitation at fourteen Greenland AWS before presenting an analysis of long-term precipitation time series.

This study sets out to obtain a robust precipitation dataset for Greenland, including precipitation phase, based on Greenland weather station observations. To that end, we apply different correction methods to the precipitation time series, distinguishing different gauge and precipitation types. These results are used to evaluate the regional climate model RACMO2.3p2, which is then used to present Greenland-wide maps of rainfall and snowfall (1958–2018). The in situ precipitation observations and the climate model are described in section 2, followed by a description of precipitation phase identification schemes and correction methods in section 3. The results including details of a case study are presented in section 4, and section 5 presents a discussion on uncertainties and some perspectives.

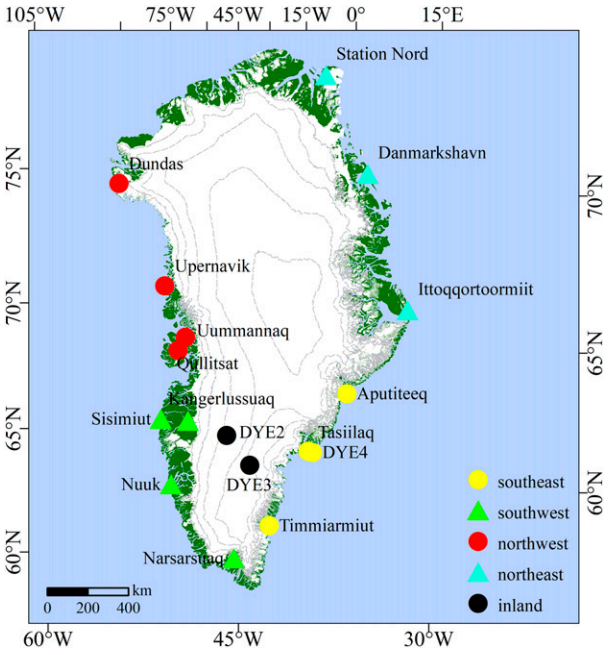

FIG. 1. The precipitation stations used in this study. Circles represent AWS and triangles represent manual precipitation stations. The symbol color represents the region a station was assigned to, as indicated in the bottom right. Background colors dark green represent ice-free tundra and white glaciated area. Dashed lines are 500 m elevation contours.

2. Data

a. *In situ observations*

Precipitation data were obtained from AWS and staffed stations operated by the DMI (Cappelen 2020) (Fig. 1). The staffed stations use Hellmann precipitation gauges (orifice area = 200 cm^2), globally one of the most widely used precipitation gauges (Sevruk and Klemm 1989). The gauges are placed with their orifices 3 m above the ground level and are equipped with a Nipher shield to reduce undercatch (Allerup et al. 1998). The AWS use the automatic Pluvio gauges, which have the same opening area, distance above the ground, and Nipher shield as the Hellmann gauges. We selected precipitation records from 17 DMI stations (11 AWS and 6 staffed stations, see Fig. 1), with relatively few data gaps and providing reasonable coverage of Greenland's coastal regions. Data of three additional stations, DYE-2, DYE-3, and DYE-4 are obtained from the Data Processing Division, Environmental Technical Applications Center of the U.S. Air Force, as "U.S. Air Force" type. Most stations are located near sea level in the ice-free coastal area, but DYE-4 is located on an elevated cape on Kulusuk Island, while DYE-2 and DYE-3 are situated at the elevated surface of the inland ice sheet.

Technical details of the stations and climate time series used in this study, including location, data period, and gauge type, are provided in Table 1 (Cappelen 2020). The six staffed stations are located in southwest and northeast Greenland (triangles in Fig. 1: after 2012, the staffed station in Nuuk was replaced by an AWS) and report 12-h accumulated precipitation. The AWSs are situated in northwest and southeast Greenland (circles in Fig. 1) and had different degrees of automation over time, which has had consequences for the way parameters are observed and for the quality of the data series (WMO 2008).

b. *RACMO2*

RACMO2 is developed and maintained at the Royal Netherlands Meteorological Institute (Koninklijk Nederlands Meteorologisch Instituut) (KNMI; Van Meijgaard et al. 2008). The polar version of RACMO2 was developed by the Institute for Marine and Atmospheric Research (IMAU), Utrecht University, to specifically simulate the surface mass balance over land ice in the Polar regions (Noël et al. 2018). The latest

TABLE 1. Details of precipitation stations: location, available data periods, gauge type, time resolution, and unit.

Station name[a]	Lat (°N)	Lon (°W)	Elevation (m MSL)	Available data period	Gauge type	Time resolution (h)	Unit
Aputiteeq	67.78	32.30	20	1958–79	Pluvio	12	0.1 mm
Tasiilaq	65.60	37.63	36	1958–2012	Pluvio	12	0.1 mm
DYE-4	65.52	37.17	329	1982–87	Pluvio	12	0.1 mm
Timmiarmiut	62.53	42.13	10	1958–79	Pluvio	12	0.1 mm
Mitt. Sisimiut	66.95	53.72	10	2014–18	Hellmann	24	1 mm
Kangerlussuaq	67.00	50.80	50	2014–18	Hellmann	24/12[b]	1 mm
Narsarsuaq	61.17	45.42	26	2014–18	Hellmann	24	1 mm
Nuuk	64.18	51.73	54	1999–2012	Pluvio	12	0.1 mm
Dundas	76.57	68.80	21	1961–74	Pluvio	12	0.1 mm
Upernavik	72.78	56.17	63	1958–81	Pluvio	12	0.1 mm
Uummannaq	70.67	52.12	39	1961–65	Pluvio	12	0.1 mm
Qullitsat	70.05	52.85	2	1961–66	Pluvio	12	0.1 mm
Station Nord	81.60	16.67	36	2014–18	Hellmann	24	1 mm
Danmarkshavn	76.77	18.67	11	2014–18	Hellmann	24	1 mm
Ittoqqoortoormiit	70.48	21.95	65	2014–18	Hellmann	24	1 mm
DYE-2	66.48	46.28	2332	1982–87	Pluvio	12	0.1 mm
DYE-3	65.18	43.83	2652	1982–87	Pluvio	12-	0.1 mm

[a] DYE stations are U.S. Air Force type.
[b] Mitt. Kangerlussuaq observed 12-h accumulated precipitation. In 2016 this changed to 24-h accumulated precipitation. In 2017 it changed again to 12 h.

version (RACMO2.3p2) includes a new cloud scheme allowing for ice super saturation (Noël et al. 2015; Tompkins et al. 2007). The update results in improved relative contributions of rainfall and snowfall to the total precipitation flux (Noël et al. 2018). In the update, the cloud water-to-snowfall conversion coefficient remains constant for liquid (>0°C) and mixed phase clouds (−23° to 0°C), whereas it decreases with temperature for ice clouds (<−23°C), resulting in changes in snowfall production (ECMWF 2008; Van Wessem et al. 2014). Given the uncertainties in the wind speed reduction to gauge height and the identification of precipitation phase using near-surface meteorological observations, previous studies concluded that the errors of daily corrections are essentially random and tend to cancel out when monthly totals are computed (Yang et al. 1999). That is why for comparison with observed precipitation, here we use monthly output of the RACMO2.3p2 run at 5.5 km resolution, notably, total monthly precipitation and snow/rainfall for the period 1958–2018 (Noël et al. 2018). This version is forced at the lateral boundaries by ERA-40 (1958–78) and ERA-Interim (1979–2018).

3. Methods

a. Preprocessing of precipitation observations

The DMI precipitation dataset has been quality controlled by the data provider, homogenized using the standard normal homogeneity test (Steffensen et al. 1993; Steffensen 1996), and compared with neighboring station records where data are available (Cappelen 2013). Before application of the data to identify the precipitation phase, here the following additional data processing steps were made:

1) We ignore precipitation amounts flagged as ''−1,'' which, according to the DMI Technical Report, applies to observations more than 0 mm, but less than 0.1 mm accumulated precipitation.
2) Small gaps for the high temporal (1 h) resolution stations in the coastal dataset were filled using linear interpolation. This applies mainly to temperature and relative humidity data after 2013, which are used in the identification of precipitation phase schemes and correction methods.
3) After the DMI quality control, data coverage for most stations reached >98%. All remaining potentially erroneous data (e.g., outliers) have been carefully inspected, corrected, or removed.
4) Monthly totals for comparison with RACMO2.3p2 are calculated only for months without missing daily totals.

b. Precipitation phase identification schemes

Near-surface (1.5 or 2 m) air temperature data are usually available together with precipitation observations, and therefore widely used for the identification of precipitation phase: liquid (rain), solid (snow), or mixed phase. These include simple temperature thresholds (Hock and Holmgren 2005; Loth et al. 1993; Berghuijs et al. 2014; Lindström et al. 1997; Yang et al. 1997) or more elaborate wet-bulb temperature schemes (Ding et al. 2014; Yamazaki 2001). The seven empirical methods to identify precipitation phase used in this study are listed in Table 2.

c. Precipitation undercatch correction

1) STAFFED PRECIPITATION STATIONS

Because these devices are used worldwide, many experimental studies on the Hellmann gauges have been conducted (Sevruk 1982; Günther and Graf 1991; Milkovic 1989). To assess national methods of measuring solid precipitation, the WMO Solid Precipitation Measurement Intercomparison was

TABLE 2. Precipitation phase identification schemes used in this study, with their acronyms as used in the text and the region for which they were originally developed. Highlighted in boldface font are the two wet-bulb temperature-based methods that are detailed in appendix A.

Scheme (acronym)	Region	Time period	Threshold
Hock and Holmgren (2005) (HH)	Storglaciären (Sweden)	1993–94	0.5°, 2.5°C
Loth et al. (1993) (LO)	Germany	1975–80	−1°, 4°C
Berghuijs et al. (2014) (BE)	North Pole region	1875–2008	1°C
Lindström et al. (1997) (LI)	Sweden	1969–89	−1°, 1°C
Yang et al. (1997) (YA)	Yershov, Uralsk (Russia)	1978–83	2.2°C
Yamazaki (2001) (YZ)	**Eastern Siberia (Russia)**	**1986–94**	**Wet-bulb *T* 1.1°C**
Ding et al. (2014) (DI)	**China**	**1951–79**	**Wet-bulb *T* probability**

started in the Northern Hemisphere winter of 1986/87 (WMO 1993). The WMO intercomparison method for precipitation gauges has been applied in various forms and at different sites, also for Hellmann gauges (Rubel and Hantel 1999; Yang et al. 1999; Bogdanova et al. 2002; Michelson 2004; Milkovic 2002; Yang et al. 2005). Precipitation observations from Hellmann gauges should be corrected for wetting losses, trace precipitation, evaporation loss and wind-induced errors caused by the wind field deformation over the gauge orifice (Sevruk and Hamon 1984; Yang et al. 1999). Studies performed in northern Canada and Alaska indicated that trace precipitation and wetting loss corrections were important in high latitudes (Metcalfe and Goodison 1993). According to Mernild et al. (2015), the mean correction factor was 1.47 ± 0.12 for 14 Greenlandic stations, ranging from 1.48 to 1.74 in the northern part of coastal Greenland and from 1.27 to 1.56 in the southern part. Yang et al. (1999) use Greenland data from the U.S. National Climatic Data Center to show that wind-induced undercatch represents the largest error, and report the correction factors for 24-h time resolution Hellmann gauge measurements for Greenland stations as follows:

$$P_c = K(P_g + \Delta P_w + \Delta P_e) + \Delta \mathrm{Pt}, \tag{1}$$

where P_c is the corrected precipitation; P_g is the gauge-measured precipitation; ΔP_w and ΔP_e are wetting loss and evaporation loss, respectively; and ΔPt is the trace precipitation. According to Yang et al. (1999), wetting loss, evaporation loss, and trace amounts result in a precipitation measurement error of less than 0.10 mm, which is below the resolution of the Hellmann gauge measurement. For any given trace day regardless of the number of trace observations reported, a value of 0.10 mm was assigned and added to the monthly total.

In Eq. (1), K is the correction coefficient for wind-induced errors. When daily wind speed at the gauge height was available, the daily catch ratio (CR) for the Nipher-shielded Hellmann gauges was calculated using the regression equations, Eqs. (3)–(5), for snow, sleet, and rain, after which K was calculated using Eq. (2):

$$K = 100/\mathrm{CR}, \tag{2}$$

$$\text{CR snow: } 100 - 11.95\,\mathrm{Ws} + 0.55\,\mathrm{Ws}^2 \quad (0 \le \mathrm{Ws} \le 6.5\ \mathrm{m\,s^{-1}}), \tag{3}$$

$$\text{CR sleet: } 100 - 8.16\,\mathrm{Ws} + 0.45\,\mathrm{Ws}^2 \quad (0 \le \mathrm{Ws} \le 6.5\ \mathrm{m\,s^{-1}}), \tag{4}$$

and

$$\text{CR rain: } 100 - 4.37\,\mathrm{Ws} + 0.35\,\mathrm{Ws}^2 \quad (0 \le \mathrm{Ws} \le 6.5\ \mathrm{m\,s^{-1}}), \tag{5}$$

where Ws is daily mean wind speed (m s^{-1}) at the gauge height. The following equation is used to estimate wind speed at gauge orifice height (3 m) using the observed 10 m wind speed (Goodison et al. 1998):

$$\mathrm{Ws} = [\log(h/z_0)/\log(H/z_0)]W_H, \tag{6}$$

where Ws is the wind speed at the height of the gauge orifice; h is the height (m) of the gauge orifice above the ground; z_0 is the roughness length, chosen to be 0.0003 m for winter, spring, fall and 0.0025 m for summer; H is the height of the wind speed measuring instrument above the ground (m); and W_H is the wind speed measured at the height H above the ground (m s^{-1}).

2) AUTOMATIC WEATHER STATIONS

For the AWSs, Michelson (2004) used the dynamic correction model (DCM; Førland et al. 1996) derived from precipitation measurements from gauges in the Baltic Sea drainage basin. This correction method was developed by the National Meteorological Services of the Nordic countries for application to 12-h precipitation gauge observations available from AWS. They used a correction factor K for different phases of precipitation on a gauge coefficient:

$$P_c = K(P_g + \Delta P_w + \Delta P_e), \tag{7}$$

where K is the correction factor for wind; P_g is measured precipitation; ΔP_w and ΔP_e are wetting loss and evaporation loss (according to appendix Tables B1 and B2, respectively). Calculation of K is based on the following equations:

(i) For liquid precipitation

$$K_l = \exp[-0.001\,01\ln(I) - 0.012\,177\,\mathrm{Ws}\ln(I) + 0.034\,331\,\mathrm{Ws} + 0.007\,697 + c], \tag{8}$$

where I is the rain intensity (mm h^{-1}), c is the gauge coefficient (appendix Table B3), and Ws the wind speed (m s^{-1}) at gauge height.

(ii) For solid precipitation

$$K_s = \exp(\beta_0 + \beta_1 \mathrm{Ws} + \beta_2 T + \beta_3 \mathrm{Ws} T) \quad \text{for} \quad 1 < \mathrm{Ws} < 7\ \mathrm{m\ s^{-1}}, \tag{9}$$

$$K_s = 1 \quad \text{for} \quad \mathrm{Ws} \le 1\ \mathrm{m\ s^{-1}}, \tag{10}$$

where β_i are gauge coefficients in (appendix Table B3), Ws is the wind speed at gauge height ($\mathrm{m\ s^{-1}}$), and T is the temperature (°C). In case $\mathrm{Ws} > 7\ \mathrm{m\ s^{-1}}$ we apply Eq. (9) for a wind speed of $7\ \mathrm{m\ s^{-1}}$.

(iii) For mixed precipitation

$$K_m = (r_l K_l + r_s K_s)/(r_l + r_s), \tag{11}$$

with K_l and K_s the correction factors for liquid and solid precipitation, and r_l and r_s are the precipitation amounts in liquid and solid form, respectively.

Based on these expressions we calculate the 12-h time resolution correction factor for solid and liquid precipitation, after applying all precipitation phase identification schemes listed in Table 2. Note that the DCM for solid precipitation was based on a dataset where wind speed at gauge height $\mathrm{Ws} \le 7\ \mathrm{m\ s^{-1}}$ and $T \ge -12$°C, which makes the validity of this equation unknown for stronger winds and/or lower temperatures (Michelson 2004). For the rainfall correction equations, there are no thresholds for wind speed and temperature, so on windy days we expect the uncertainty for the rainfall correction to be smaller than that for the snowfall correction.

d. Elevation calibration

We correct RACMO2.3p2 precipitation phase for not accurately resolving the terrain elevation at the gauge locations at 5.5 km resolution, using the four nearest model grid points. Rain fractions from these grid points are regressed against elevation, and a correction is then applied to account for the elevation error. This yielded corrections in absolute rainfall fractions ranging from 9% at DYE-4 (elevation difference: 278 m MSL), and 0.1% at Dundas (elevation difference: 6 m MSL).

e. Definition of rainfall fraction and rainfall totals

In this study, we define rainfall fraction as the ratio of cumulative rainfall and cumulative total precipitation summed over the available years with semicomplete observations (Table 3). This approach differs from averaging annual rainfall fractions, but the difference is small. Based on RACMO2.3p2 output applied to station location and observational period, the difference in percentage point is smaller than 1% everywhere, with the exception of Danmarkshavn (1.1%, see Table 3). To determine the cumulative quantities of rainfall and total precipitation and hence rainfall fraction from observations, all available months were used, also from years where a small number of months was missing. In contrast, annual total rainfall is based on averaging only complete years.

f. Workflow and uncertainty analysis

The workflow proceeded as follows: first, for each station we calculated solid and liquid precipitation amounts at the original time resolution using the seven precipitation phase identification schemes. Next, we corrected these solid/liquid precipitation amounts for wind, wetting and evaporation effects using the expressions presented above. We then calculated the average and the standard deviation of the seven resulting time series, the latter to be used as a measure for the observational uncertainty in rain fraction. In addition, we performed a sensitivity analysis in which we varied the observed wind speed and temperature to see how it affects the correction factors. Finally, we compare monthly totals with the (elevation corrected) RACMO2.3 model output of rainfall and snowfall rate at the station locations, and calculated the correlation coefficient, bias, and RMSE. We define five Greenland sectors to facilitate the interpretation (Fig. 1).

TABLE 3. Station rainfall fraction (%) from RACMO2.3p calculated in two different ways: as the ratio of cumulative totals or the average of annual fractions over the period of observations (first column).

Station name	Available data period	Ratio of cumulative totals (%)	Avg of annual fractions (%)
Aputiteeq	1958–79	23.0	23.1
Tasiilaq	1958–2012	27.5	27.4
DYE-4	1982–87	34.1	34.2
Timmiarmiut	1958–79	25.6	24.8
Mitt. Sisimiut	2014–18	32.6	32.5
Kangerlussuaq	2014–18	53.9	53.8
Narsarsuaq	2014–18	56.8	56.9
Nuuk	1999–2012	43.3	43.3
Dundas	1961–74	22.6	22.8
Upernavik	1958–81	28.1	27.6
Uummannaq	1961–65	27.6	28.0
Qullitsat	1961–66	29.8	29.9
Station Nord	2014–18	4.5	4.5
Danmarkshavn	2014–18	12.5	13.6
Ittoqqoortoormiit	2014–18	30.0	30.3
DYE-2	1982–87	0.8	1.0
DYE-3	1982–87	0.3	0.3

4. Results

To illustrate the three-step procedure [(i) identification of precipitation phase, (ii) precipitation correction, and (iii) RACMO2.3 evaluation for monthly totals], in this section we present two case studies using observations from the AWS in Aputiteeq in southeast Greenland (section 4a) and from the staffed station Mitt. Sisimiut in southwest Greenland (section 4b). Then we perform a full model evaluation using all stations (section 4c), and finally we discuss the climatological total precipitation and rainfall conditions with the corrected observed and modeled results (section 4d).

a. Aputiteeq: Case study of an AWS

The southeast region in which this station is located is characterized by high precipitation totals (Ettema et al. 2009) and relatively moderate temperatures, resulting in a significant rainfall fraction. Figure 2 shows the result of step (i), that is, the uncorrected 12-h precipitation totals using the seven precipitation

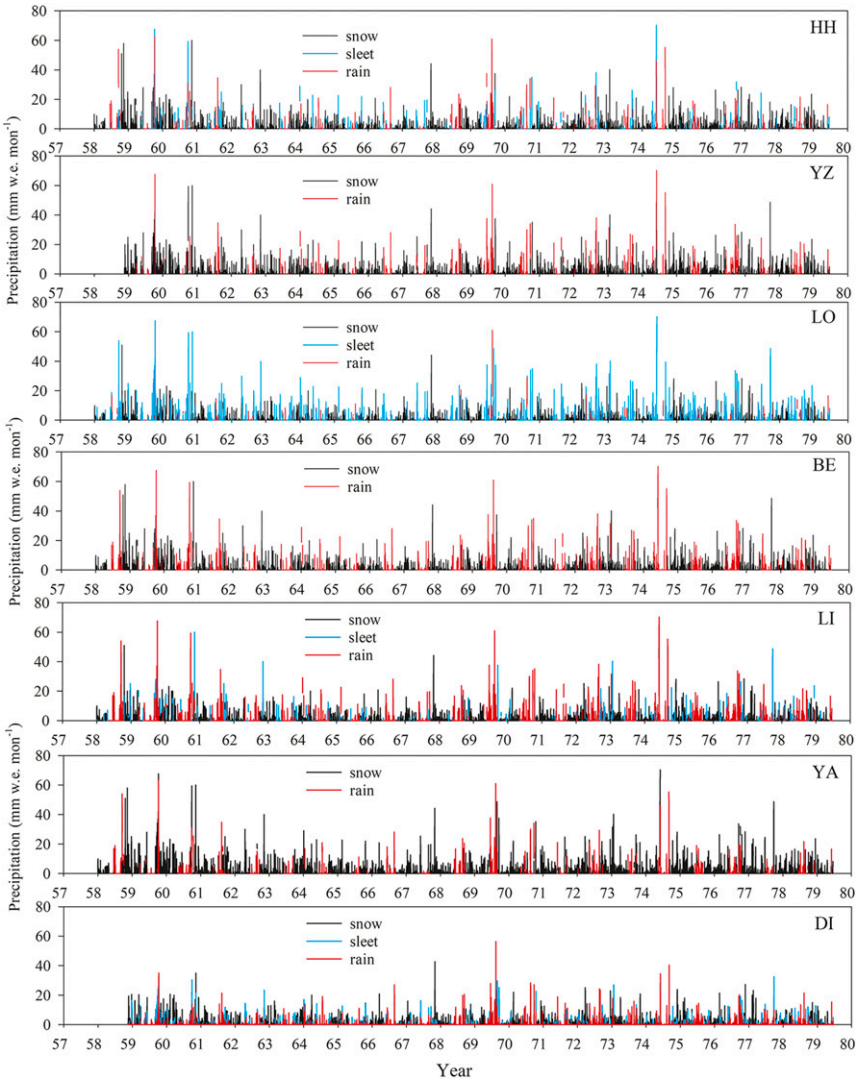

FIG. 2. Aputiteeq uncorrected 12-h totals of solid (snow), mixed phase (sleet, only when method provides this), and liquid (rain) precipitation, using seven precipitation-phase identification schemes (Table 2). Identification scheme acronyms (top-right corner) are explained in Table 2.

phase/type identification schemes (Table 2, method abbreviation in top right of each plot) for snowfall, mixed-phase precipitation (sleet, only if the method provides) and rainfall. The fraction of liquid precipitation is high at this station, but obviously varies between the different schemes. For instance, for the method using a simple 1°C threshold (BE), the 21.5-yr cumulative (January 1958–June 1979) rainfall is 6.8 m and cumulative snowfall 10.1 m. Using a threshold of 1.1°C for the wet-bulb temperature (YZ) yields a cumulative rainfall of 4.8 m and cumulative snowfall of 11.2 m. For all seven methods, the cumulative rainfall ranges between 8% (LO and 55% sleet) and 40% (DI, LI, BE) of the total precipitation. The intermediate schemes (HH, YZ) produce rainfall percentages between 19% (HH) and 30% (YZ). For the near surface temperature threshold method, the total cumulative precipitation from January 1958 to June 1979 is 16.9 m while for the wet-bulb temperature probability method it is 16.1 m, as humidity data are missing for some time periods.

Next [step (ii)] we apply the correction factors for solid (K_s) and liquid (K_l) precipitation (the latter including sleet) to these time series. Note that different precipitation separation schemes will lead to differences in average solid and liquid correction factors, because differences are introduced in the meteorological conditions during the precipitation events per type. Figure 3 shows the 12-h correction factors for Aputiteeq. Correction factors are especially large for snow (solid precipitation): at higher wind speeds, K_s can reach ~40, while the correction for liquid precipitation (K_l) is lower and more constant. The average values of K_s vary from 2.86 (LO) to 2.56 (DI) while the values for K_l vary from 1.17 (HH) to 1.21 (BE).

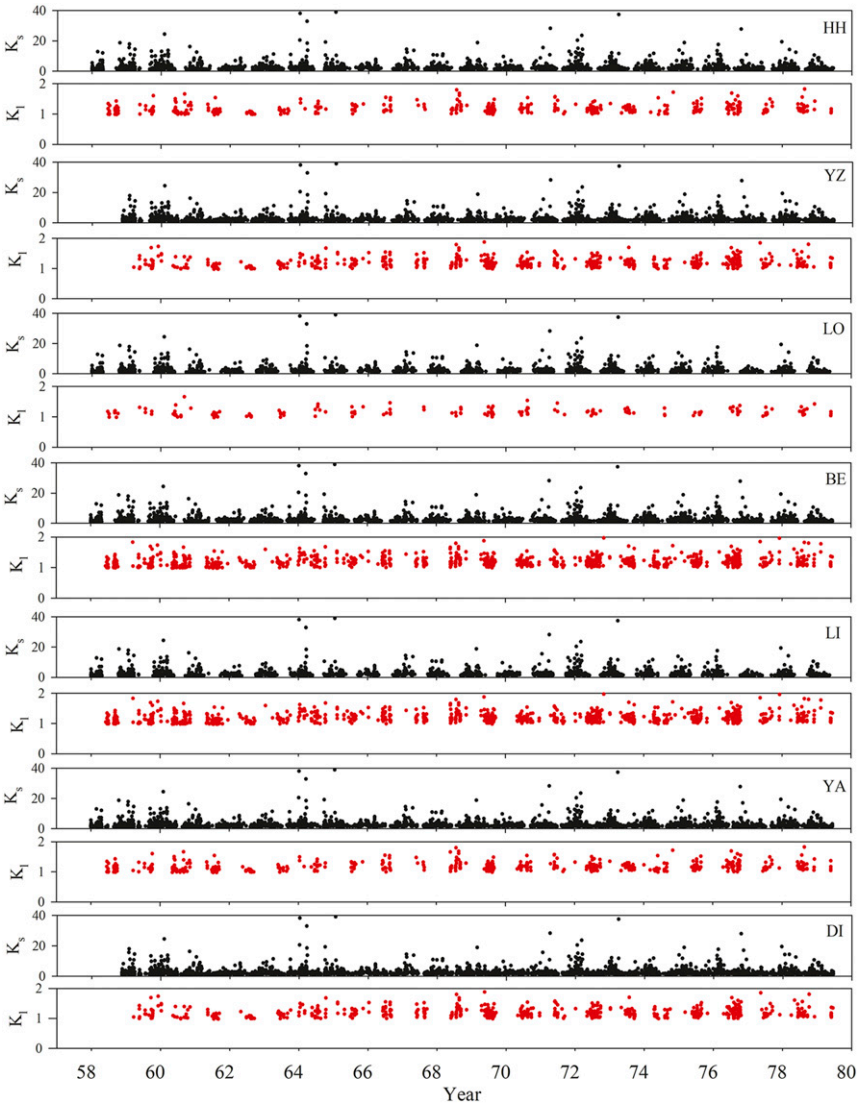

FIG. 3. Aputiteeq 12-hourly solid (K_s) and liquid (K_l) correction factors for the different precipitation-type identification schemes. Identification scheme acronyms (top-right corner) are explained in Table 2.

For Aputiteeq, the overall average values over all seven methods are 2.75 ± 0.10 for K_s and 1.18 ± 0.02 for K_l.

Seven time series for Aputiteeq snowfall, sleet (if available) and rainfall were obtained by applying the 12-h correction factors to the 12-h precipitation totals. As an example, Fig. 4 shows the resulting corrected 12-h snowfall (Fig. 4a) and rainfall (Fig. 4b) for scheme BE at Aputiteeq. Corrections applied at a shorter time scale are expected to produce better results since the 12-h mean wind speeds may not be representative of wind conditions during precipitation, but unfortunately this information is not available.

Next [step (iii)] we use the corrected precipitation observations to evaluate the regional climate model RACMO2.3. To reduce noise, we calculated cumulative monthly snowfall and rainfall total based on the corrected 12-h data. For each of the seven precipitation phase identification schemes (Table 2), Fig. 5 compares Aputiteeq with RACMO2.3p2 monthly total precipitation in the left and rainfall in the right column. Correlation coefficients for total precipitation vary between 0.73 and 0.82 and between 0.49 and 0.90 for rain, but between 0.73 and 0.90 if scheme LO is excluded. The deviating LO rainfall results suggest that a 4°C upper threshold is not suitable, at least for station Aputiteeq. RACMO2.3p2 appears to generally overestimate total precipitation for this station, yet at the same time it fails to reproduce some of the very high monthly totals that emerge from the correction procedure for snow.

Figure 6 compares the Aputiteeq time series (1958–79) of observed (corrected) monthly total precipitation, snowfall, and rainfall, including the standard deviation (std dev) based on the differences between the seven precipitation phase identification

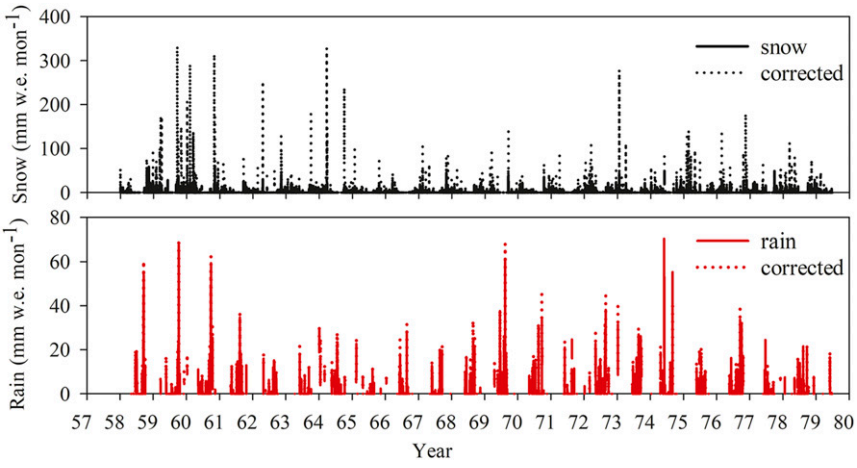

FIG. 4. Aputiteeq corrected 12-hourly (top) solid and (bottom) liquid precipitation for scheme BE.

schemes, with model results from RACMO2.3p2. Since there is no clear reason to prefer one scheme over the other, in the remainder we will present the average of the seven different schemes and the uncertainty as the standard deviation. Especially rainfall is well represented, with most of the differences in total precipitation deriving from the snowfall estimates, which we ascribe in part to the less certain correction procedure. The average difference during 1958–79 for snowfall is 37 mm water equivalent (w.e.) month^{-1} and for rainfall 11 mm w.e. month^{-1}. Interestingly, both in the observations and in the model, rainfall peaks in late summer (August or September), which could be explained by a combination of increased precipitation and still relatively high temperatures. For Aputiteeq, the mean standard deviation of the seven identification schemes is 19 mm w.e. month^{-1} for total precipitation, 29 mm w.e. month^{-1} for snowfall, and 11 mm w.e. month^{-1} for rainfall, that is, comparable to the model–observation differences.

Figure 7 compares modeled and observed yearly totals for station Aputiteeq, using the standard deviation based on seven identification schemes of precipitation phase to quantify the observational error. RACMO2.3 generally overestimates annual precipitation totals at Aputiteeq, both solid and liquid, although for most years the difference remains close to the observational uncertainty (vertical error bars in Fig. 7). For this period (1958–79), observed and modeled average total precipitation are 1552 ± 234 mm w.e. yr^{-1} and 2087 mm w.e. yr^{-1}, respectively (error equals the standard deviation in the annual totals) while observed and modeled average rainfall are 359 ± 104 mm w.e. yr^{-1} and 494 mm w.e. yr^{-1}. Note how the correction of the observations has improved the correlation, from 0.70 to 0.78 for total precipitation and from 0.71 to 0.89 for rainfall. Time series of the other stations show similar agreement (see Figs. S1–S7 in the online supplemental material for the other automatic weather stations).

b. Mitt. Sisimiut: Case study of a staffed precipitation station

This coastal site in southwest Greenland is characterized by medium precipitation totals (Ettema et al. 2009) and relatively mild conditions, resulting in a significant rainfall fraction. Staffed precipitation stations use the shielded Hellman gauge (Table 1) and report 24-h accumulated precipitation. Figure 8 evaluates RACMO2.3p2 using the corrected observed total monthly precipitation using the seven precipitation phase identification schemes for station Mitt. Sisimiut (see Figs. S8–S12 for the other staffed stations). Again, the model results agree well with the observations, with correlation coefficients for total precipitation between 0.79 and 0.81. The correction method results in some total daily precipitation values that are much higher than modeled at this station, resulting in some outlying monthly values. This could be an effect of limited model resolution in combination with rugged topography; notably, the study of Ettema et al. (2009) comparing simulations of RACMO2.1 at various resolutions reveals a direct relation between the grid cell area and the total precipitation over the GrIS. But overall, it appears that corrected Hellmann gauge precipitation observations, as used on the staffed precipitation stations, provide robust precipitation results for southwest and northeast Greenland. Other experimental studies confirm the high catch ratio of the shielded Hellmann gauge: on average, the unshielded Hellmann gauge catches 60% of snowfall and 83% of rainfall, and the shielded Hellmann gauge 77% and 86%, respectively (WMO 2008).

To illustrate the typical temporal variability and (dis) agreement of the resulting time series for the staffed stations, Fig. 9 compares Mitt. Sisimiut corrected time series (2014–18) of monthly accumulated total precipitation, snowfall, and rainfall with RACMO2.3p2. The blue bars represent the std dev from the seven precipitation phase identification schemes, with values on the right axis. In both observed and model time series for this station we see extreme month-to-month variability. Observed (corrected) monthly total precipitation ranges from <1 to 160 mm w.e. month^{-1}. The temporal variability and absolute values at this station are generally well captured by RACMO2.3p2, although significant differences are evident for individual months. Time series of the other

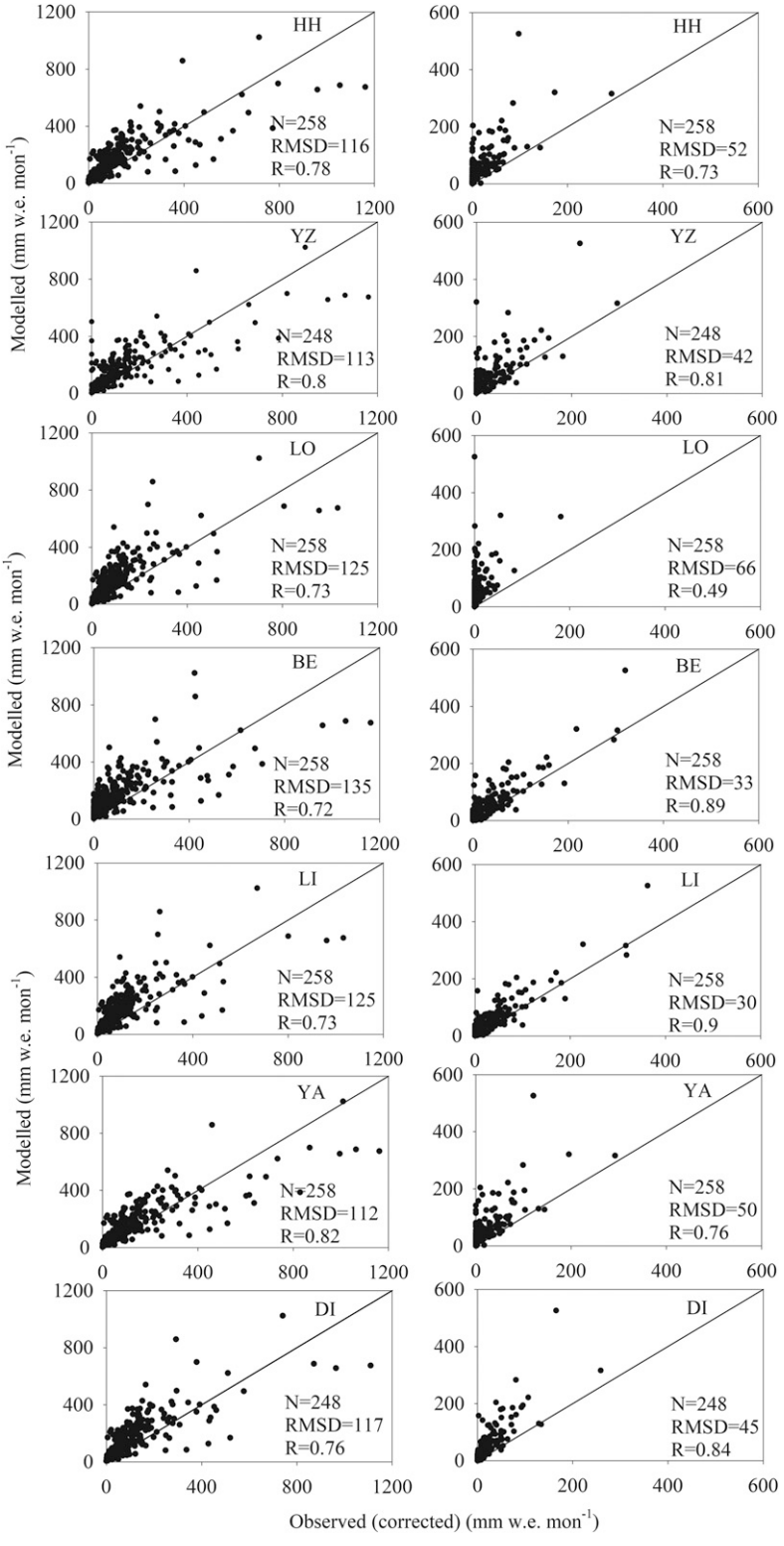

FIG. 5. Aputiteeq monthly totals (mm w.e. month^{-1}) of modeled (RACMO2.3p2) vs observed (corrected) (left) total precipitation and (right) rain for seven precipitation-phase identification schemes (Table 2). RMSD = root-mean squared deviation, N = number of months, R = linear correlation coefficient.

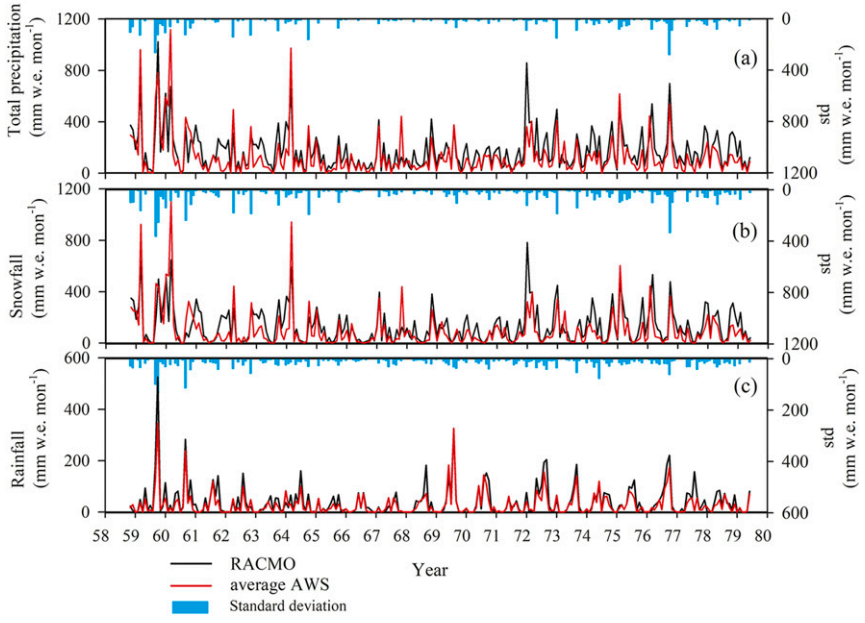

FIG. 6. Aputiteeq monthly time series for RACMO2.3p2 and average corrected AWS results with seven precipitation identification schemes of precipitation-phase (a) total precipitation, (b) snowfall, and (c) rainfall. Blue bars represent the standard deviation of the seven schemes.

stations show similar agreement and are presented in the Figs. S13–S17.

c. *Model evaluation using all stations*

Figure 10 shows the performance of RACMO2.3p2 in terms of root-mean-squared deviation (RMSD) and correlation for all considered stations, based on all available monthly values, where the observations represent the average and the error bar the standard deviation of the seven precipitation phase identification schemes. Almost all stations show higher correlation for rainfall than for total precipitation. For total precipitation, most of the manual (staffed) stations consistently show high correlations. The differences among the methods for the staffed stations (southwest and northeast regions) is relatively small, expressed by a small standard deviation. If we look at the results of the seven individual precipitation phase identification schemes (Figs. S18–S20), LI with lower and upper temperature thresholds of −1° and 1°C, respectively, shows the best agreement with RACMO2.3p2, with a low RMSE and a high correlation coefficient at most stations. The LO scheme with −1° and 4°C temperature thresholds shows generally much poorer agreement. In addition, except for station DYE-4, the total precipitation at the southern stations (southeast and southwest) appears to be better simulated than at the northern stations (northeast and northwest) (Fig. 10 and Figs S18–S20). A likely explanation is that the correction factors for precipitation decrease from 50% to 75% in the northern regions to from 20% to 40% in the southern regions, mainly because of the higher percentage of snowfall in the north (Yang et al. 1999).

The two inland stations on the ice sheet (DYE-2 and DYE-3) show the lowest correlations, both for solid and liquid precipitation. This is likely largely due to a combination of high wind speeds and low rainfall fraction at these sites resulting in a large uncertainty of the precipitation measurements. Here we note that previous work showed that RACMO2.3p2 quite accurately simulates accumulation rates over the inland ice sheet, as derived from ice cores and snow pits (Noël et al. 2018). Overall, the representation of rainfall in Greenland in RACMO2.3p2 appears adequate, making it a useful tool to further analyze spatial and temporal variability of rainfall in Greenland (see next section).

d. *Climatological total precipitation and rainfall fractions*

Figure 11 compares observed and modeled rainfall fractions (Figs. 11a,b) and average annual rainfall totals (Figs. 11c), and Fig. 12 shows the rainfall fractions in a map. Note that the observational time period for staffed stations in the southwest and northeast is 2014–18, which is more recent and also considerably shorter than the AWS time series, which cover the period 1958–1965/1987 (Table 1). Figure 11a shows the observed, corrected rainfall fractions for each of the seven precipitation phase identification schemes. For the southwestern stations, the Ding et al. (2014) wet-bulb temperature scheme predicts the highest fraction liquid precipitation, but for most other stations this is true for the Lindström et al. (1997) scheme with the temperature threshold between −1° and 1°C. For most coastal stations (excluding DYE-4, which is more highly elevated), rainfall accounts for a considerable proportion of the total precipitation (Fig. 12). The highest rainfall fraction is observed at Narsarsuaq, the southernmost station in the southwest region (57 ± 8%). For the four stations in the northwest the rain fraction ranges between 18% ± 4% at Dundas and 27% ± 5% at Uummannaq, still remarkably significant fractions for stations this far north.

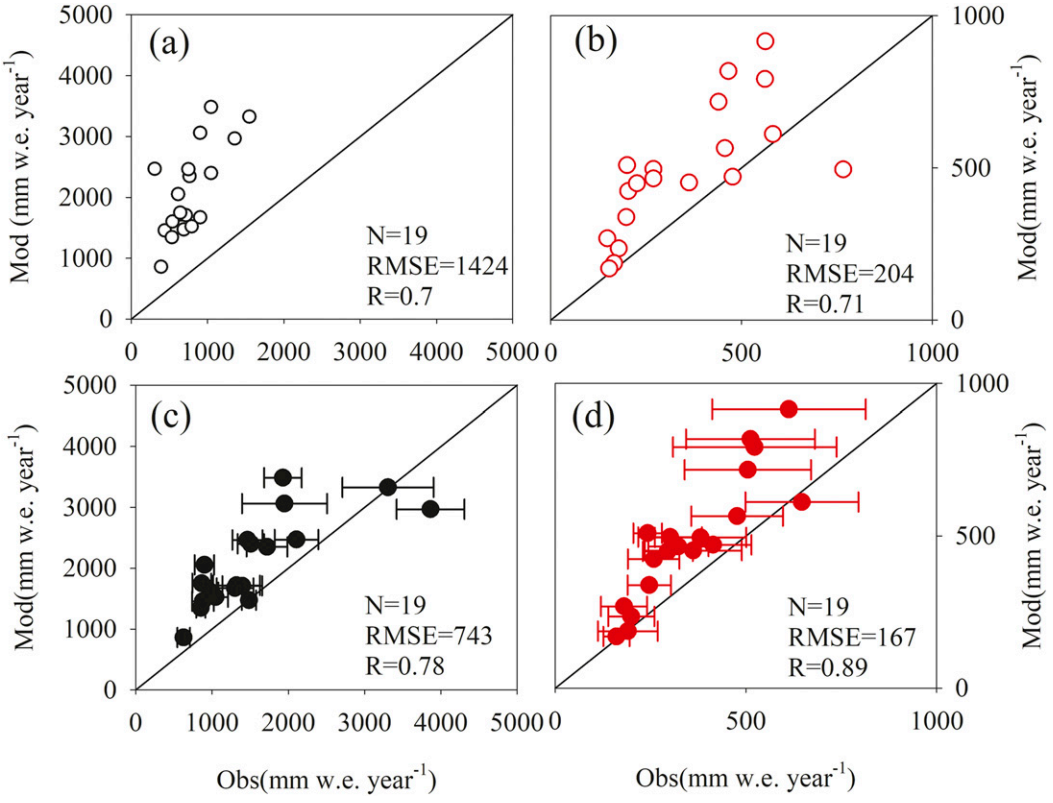

FIG. 7. (a),(b) Uncorrected and (c),(d) corrected Aputiteeq yearly totals (mm w.e. yr^{-1}) of modeled (RACMO2.3p2) vs observed (a),(c) total precipitation and (b),(d) rain. Error bars in observations represent the standard deviation of seven precipitation-phase identification schemes (Table 2). RMSE = root-mean squared error, N = number of months, R = linear correlation coefficient.

The rain fraction modeled in RACMO2.3p2 agrees with the observations generally within the uncertainty obtained from the standard deviation between different identification schemes (Fig. 11b). The largest and most significant differences between measurements and model occur for the southeast. The former DYE-4 radar station is located on an isolated cape (329 m MSL), which is poorly resolved in the 5.5-km-resolution model topography. The nearest gridpoint in the model domain has an elevation of only 51 m, and bilinearly interpolating the four nearest grid points yields an elevation for DYE-4 of 210 m, that is, still 119 m too low. Using the neighboring points to calculate the elevational gradient in rain fraction we recalculate the rainfall modeled at DYE-4. This correction was also performed for the other stations, where the elevation differences are generally small (<50 m) and the correction less significant.

Figure 11c shows corrected observed annual rainfall (mm w.e., based on complete years only) and compares it to RACMO2.3. The well-known pattern emerges of relatively wet conditions in the east to southeast, and drier conditions generally along the west and north. Rainfall is significant everywhere, with the exception of the two inland stations situated on the ice sheet. Mean annual rainfall peaks at 539 mm w.e. in Timmiarmiut. Somewhat smaller rainfall amounts are observed in the southwest, but also with significantly lower total precipitation, implying a larger rainfall fraction, for example, in excess of 50% at Kangerlussuaq, with an annual rainfall of 116 mm w.e. In the colder north, annual rainfall ranges from 34 mm w.e. at Station Nord to 196 mm w.e. at Ittoqqortoormiit.

5. Discussion and outlook

a. *Robustness of the precipitation corrections*

The quality of the snow- and rainfall totals presented here depends to a large extent on the methods to separate the liquid from the solid phase and the subsequent undercatch corrections. Table 4 shows the daily mean correction factors for solid precipitation (K_s) and liquid precipitation (K_l). The largest uncertainties reside in the correction factor for solid precipitation K_s for high wind speed conditions. Absolute snowfall corrections for most months ranged between 30%–60% in the southeast and 10%–70% in the northeast of Greenland (Fig. S21). The absolute snowfall corrections are highest in winter where they can reach 838 mm w.e. $month^{-1}$ in the southeast and 198 mm w.e. $month^{-1}$ in the northwest. Doyle et al. (2015) applied lower corrections of 33% for snow and 16% for rain for the automatic GEONOR gauge at an ice margin site, while for the manual gauge at Kangerlussuaq in the southwest region, summer corrections of 12% for snow and 4.5% for rain were applied.

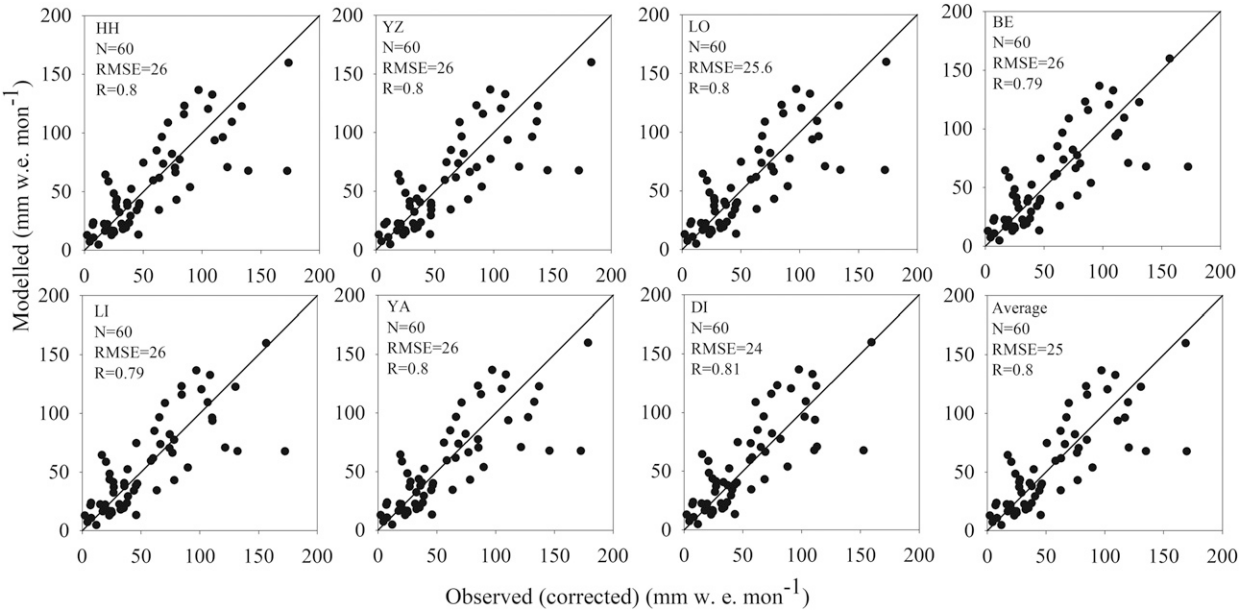

FIG. 8. Mitt. Sisimiut monthly totals (mm w.e. month^{-1}) of modeled (RACMO2.3p2) vs corrected observed total precipitation for seven precipitation-phase identification schemes (Table 2). RMSE = root-mean squared error, N = number of months, R = linear correlation coefficient.

To evaluate the sensitivity of the correction factor to climate conditions, a number of tests have been carried out on the data of the AWS Aputiteeq. The first test determines the influence of perturbed wind speed on K_s, by increasing all 12 h values by +1, +2, +3, +5, and +10 m s^{-1}, keeping temperature unchanged (Fig. 13). Assuming wind speed unchanged, the influence of temperature on K_s is pronounced. The variation in the correction factor for liquid precipitation K_l is much smaller with values between 1.2 and ~2.0 with for wind speed, whereas it remains between 1.1 and ~1.2 for temperature. These results

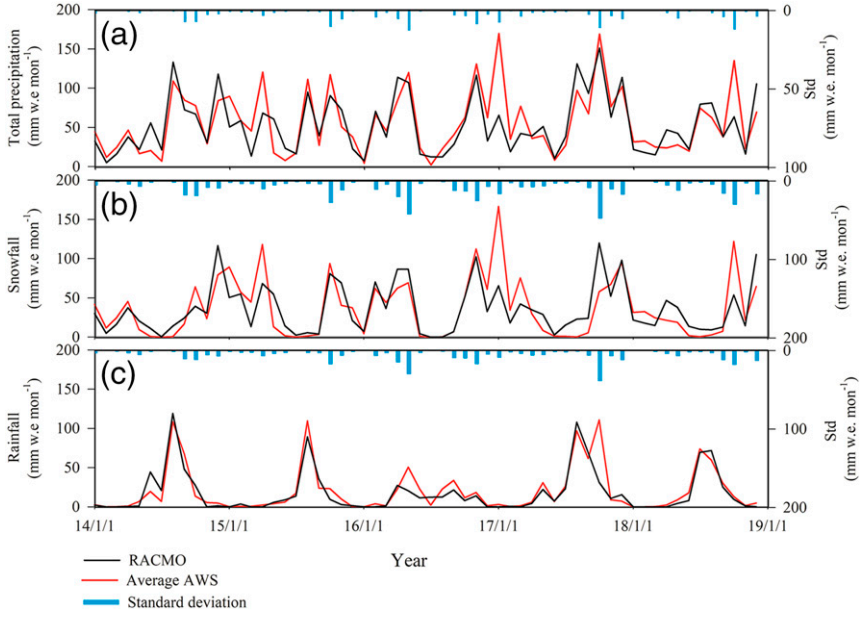

FIG. 9. Mitt. Sisimiut time series of monthly total precipitation of corrected observations averaged over the seven precipitation-phase identification schemes and RACMO2.3p2 for (a) total precipitation, (b) snowfall, and (c) rainfall. Standard deviation in blue based on seven identification schemes of precipitation phase.

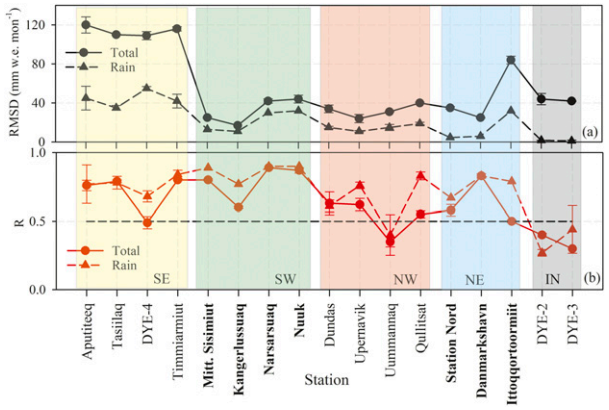

FIG. 10. (a) Root-mean squared deviation and (b) correlation coefficient for monthly total precipitation (solid line) and rain (dashed line) between (corrected) observations and RACMO2.3p2 at all stations. The manual stations are in boldface font.

confirm that liquid precipitation amounts are more robust: they depend mostly on the selected precipitation phase scheme and less on climate measurement uncertainty.

It is therefore expected that the precipitation correction for moderate wind speeds will provide reliable estimates of precipitation at Greenland observational stations. The upper threshold for wind speed for correcting wind-induced errors

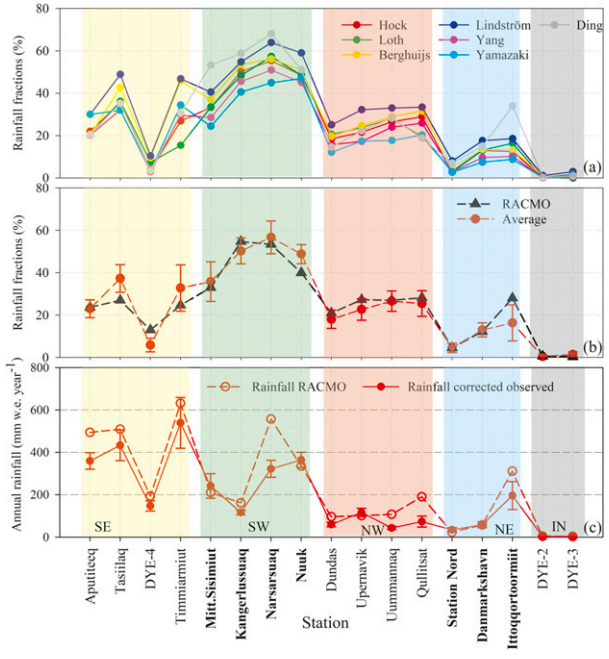

FIG. 11. (a) Observed rainfall fraction based on all cumulative monthly totals for each of the seven precipitation-phase identification schemes; (b) the average rainfall fraction of the seven precipitation-phase identification schemes with error bars representing the standard deviation and comparison to RACMO2.3p2; (c) observed total rainfall (mm yr^{-1}), based on complete years, and comparison with RACMO2.3p2.

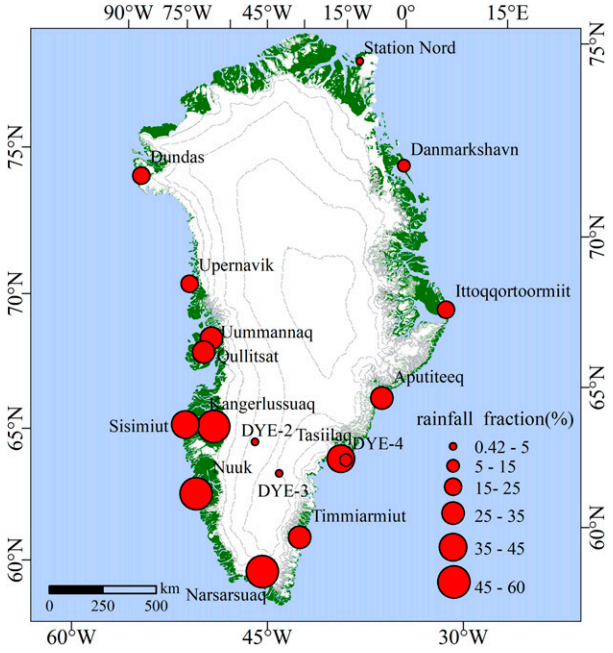

FIG. 12. Observed, corrected average rainfall fraction for all stations.

(6.5 m s^{-1} for Hellman gauges and 7 m s^{-1} for Pluvio gauges) is not often exceeded at Greenland coastal stations (Michelson 2004). Missing wind speed data present a potentially larger problem. For instance, during 1958–79 (8035 days), Aputiteeq station has a mean 12-h wind of 4.3 m s^{-1} at 10 m and 3.8 m s^{-1} at gauge height (3 m). Furthermore, on 3218 days (about 40% of the data), wind exceeded the threshold (7 m s^{-1}) or wind speed data were missing, leaving the snowfall correction uncertain. Figure 14 illustrates that for most of the stations, the

TABLE 4. Precipitation daily mean correction factors used in this study.

Station name	Mean correction factor K_s	Mean correction factor K_l
Aputiteeq	2.40	1.25
Tasiilaq	2.80	1.20
DYE-4	2.60	1.20
Timmiarmiut	2.20	1.10
Mitt. Sisimiut	1.54	1.10
Kangerlussuaq	1.46	1.17
Narsarsuaq	1.27	1.10
Nuuk	1.24	1.10
Dundas	2.30	1.40
Upernavik	2.50	1.50
Uummannaq	1.90	1.30
Qullitsat	2.10	1.20
Station Nord	1.40	1.02
Danmarkshavn	1.74	1.10
Ittoqqoortoormiit	1.48	1.10
DYE-2	2.60	1.30
DYE-3	2.50	1.40

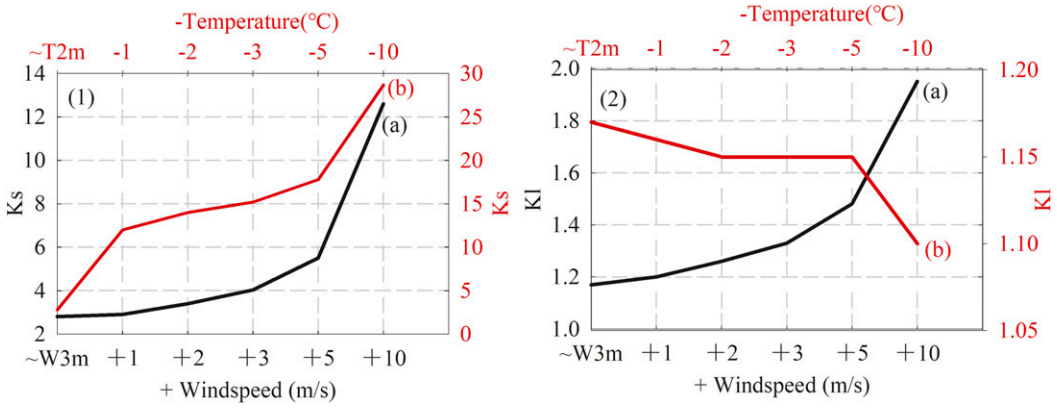

FIG. 13. Precipitation correction factor for (left) solid (K_s) and (right) liquid (K_l) precipitation for Aputiteeq, as a function of imposed perturbations on wind speed (v_g; see black line a) and as a function of temperature (T; see red line b).

availability of wind speed data exceeds 60%, and even 80% in the southwest and northeast regions.

b. *Impact of nonoverlapping periods*

In Figs. 10–12, we compare precipitation observations that have been averaged over different, sometimes nonoverlapping time periods (see Table 1). Figure 15 uses RACMO2.3p2 output to evaluate the impact this has on the average rainfall fractions at the various stations. We compare the periods 1958–2013, 2014–18, and 1958–2018. The result shows that the absolute rainfall fractions in RACMO2.3p2 do not differ significantly between these periods, except at Dundas and Ittoqqortoormiit, where the latest period in the absolute sense shows 5%–10% more rain. Furthermore, independent of the selected time period, the rainfall fraction in the southwest consistently ranks highest, and the northeast lowest (not considering the inland stations). A more detailed analysis of trends in rainfall over Greenland is outside the scope of this evaluation study and will be the topic of a future study.

c. *Using modeled precipitation to study the rain climate of Greenland*

Although station precipitation data in Greenland can be corrected to a certain extent, they still lack spatial and temporal coverage (Table 1). A physical interpolator must be used to fill these gaps. In this study we used rainfall/snowfall simulated by the regional climate model RACMO2.3p2 (1958–2018) with a horizontal resolution of 5.5 km; the evaluation shows that the model and observation-based rain fractions generally agree within the uncertainty arising from the different precipitation phase identification schemes. This provides confidence that such a model can be used to assess the variability of the rain climate of Greenland and its ice sheet in space and time.

As a first application, Fig. 16 illustrates the multiyear average (1958–2018) seasonal rainfall fractions (%) from RACMO2.3p2, obtained by dividing the cumulative totals of rain and total precipitation over 61 seasons. The model simulates large seasonal and regional variations in rainfall fraction over Greenland. In spring (MAM; Fig. 16a), rainfall fractions of up to 30% are modeled in the south and southwest. Spring and fall (Figs. 16a,c) have similar large-scale distributions of rainfall fraction, albeit with significantly higher fractions in fall in the southwest, which can be explained by the higher sea ice cover in spring to the west of Greenland. During summer (Fig. 16b), the entire coast of Greenland is sea ice free and experiences rain, the fraction ranging from 30% to 50% in the north to 70% to 100% on the western tundra. In winter (Fig. 16d), significant rain fractions are predicted only in the far south (up to 20%) and some isolated patches in the west and east. Figures 16e and 16f show the modeled mean annual total precipitation and rainfall, respectively (mm w.e. yr^{-1}). Whereas southeast Greenland

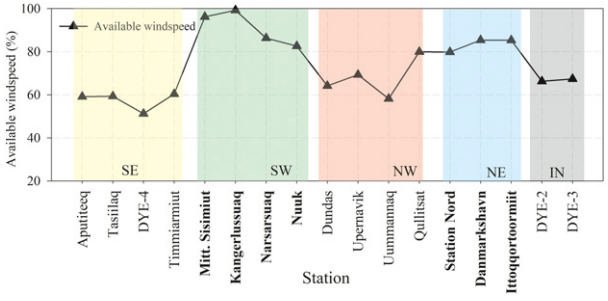

FIG. 14. Fraction of wind speed data that are both available and within the correction threshold (7 m s^{-1}).

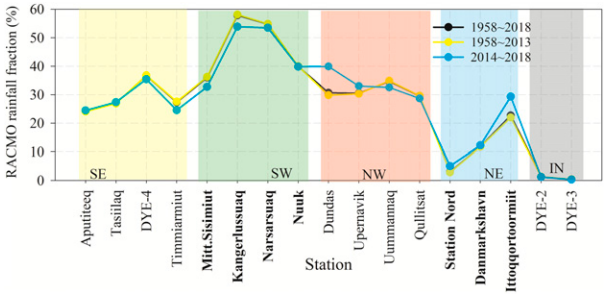

FIG. 15. RACMO2.3p2 rainfall fractions (%) at station locations for different time periods.

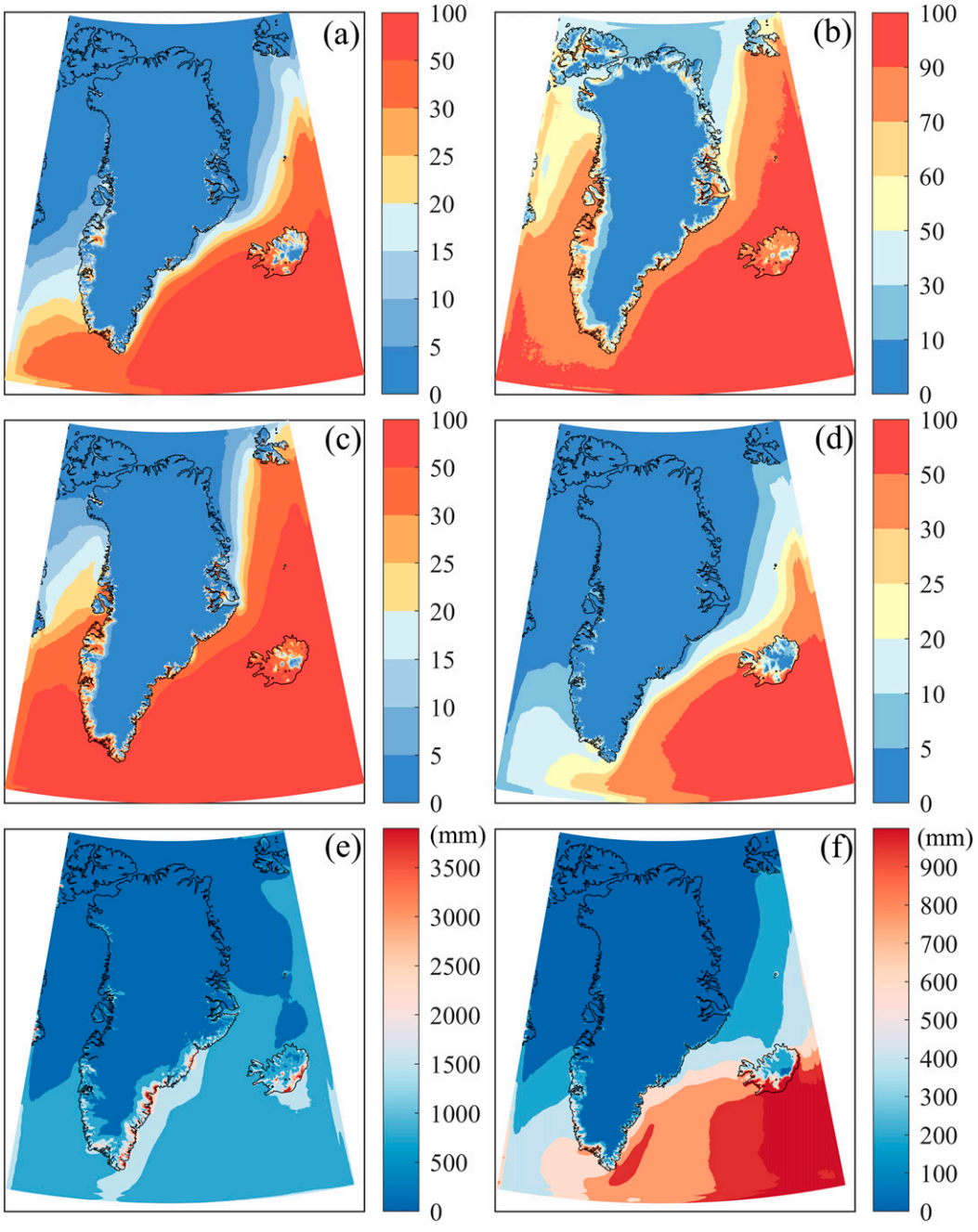

FIG. 16. RACMO2.3p2 modeled rainfall fraction (%) based on 1958–2018 cumulative totals for (a) MAM, (b) JJA, (c) SON, and (d) DJF. (e) The mean annual total precipitation. (f) The mean annual rainfall. Note the different color bars.

receives most precipitation, up to 3800 mm w.e. yr^{-1}, the extreme southwest receives most rainfall (up to 800 mm w.e. yr^{-1}).

Of special interest for the hydrology and dynamics of the marginal Greenland ice sheet is the amount of rain that falls on the lower ice sheet and narrow (floating) glacier tongues. However, as Greenland is characterized by a low-Arctic climate, it has a strong gradient in continentality between the open ocean and the ice sheet (Abermann et al. 2019). Because many of the marginal glaciological features, such as floating ice tongues, are typically not well resolved at the current model resolution of 5.5 km, quantifying this will require further statistical and/or dynamical downscaling of the modeled rainfall product to resolutions in the order of 1 km (Noël et al. 2018). This is the goal of a follow-up study. The present results show that the RACMO2.3 rain product at 5.5 km can serve as a basis for such an effort.

6. Conclusions

We present rainfall observations at 17 Greenland meteorological stations, using seven different schemes to identify precipitation phase. Further corrections for undercatch include a dynamic correction model (DCM) for AWS (Pluvio gauges) measurements (Førland et al. 1996) and a regression analysis correction method for staffed (Hellmann gauges) precipitation stations (Yang et al. 1999). We find that rainfall accounts for a considerable fraction of total precipitation in Greenland, with peak values in the southwest ranging from 36% to 57%. Especially for snowfall amounts, significant uncertainties remain in the correction for wind-induced undercatch, while the rainfall observations are relatively robust. Our results support the preliminary conclusion that rainfall fractions in Greenland are higher than previously reported (Ohmura and Reel 1991).

The corrected monthly total precipitation (snow and rain) and rainfall are compared to output of the regional climate model RACMO2.3p2. Correlations between model and observations are higher for rainfall than for total precipitation, partly because the undercatch corrections for snowfall are less certain. Although we showed that the model at 5.5 km resolution performs well with significant correlations (R = 0.3–0.9) for the coastal station locations, the horizontal and vertical gradients in rainfall are likely to be so large in Greenland that in order to accurately represent the amount of rainfall that falls on the hilly tundra, the lower ice sheet and glacier tongues, a further statistical downscaling to, for example, 1 km is deemed necessary.

Acknowledgments. This publication was supported by PROTECT. This project has received funding from the European Union's Horizon 2020 research and innovation program under a grant agreement (Grant 869304), PROTECT contribution number 20. Funding was also provided by the National Natural Science Foundation of China (Grant 41701059). The authors gratefully acknowledge data availability from the Danish Meteorological Institute (DMI), and the authors thank Brice Noël (Utrecht University) for RACMO2.3p2 data support.

Data availability statement. All the scripts of seven identification of precipitation phase schemes, correction methods, and the whole processing package are available through an email request to the authors.

APPENDIX A

Identification of Precipitation Types Scheme

a. Equations that are used by Yamazaki (2001)

$$s(\mathrm{Tw}) = 1 - 0.5\exp[-2.2(1.1 - \mathrm{Tw})^{1.3}],$$
$$r(\mathrm{Tw}) = 0.5\exp[-2.2(1.1 - \mathrm{Tw})^{1.3}]$$
$$\left.\begin{matrix}\mathrm{Tw} < 1.1^{\circ}\mathrm{C}\\ \mathrm{Tw} \geq 1.1^{\circ}\mathrm{C}\end{matrix}\right\},$$
$$\mathrm{Tw} = 0.584\mathrm{Ta} + 0.875e - 5.32$$

where Tw is the wet-bulb temperature, Ta is 2 m temperature, and e is the saturated water pressure.

TABLE B1. Wetting constants per case [mm (12 h)$^{-1}$] for synoptic gauge and precipitation phase (Michelson 2004).

Precip phase	Wetting constants
Liquid	0.14
Solid	0.10
Mixed	0.18

b. Equations that are used by Ding et al. (2014)

$$\mathrm{Tw} = \mathrm{Ta} - \frac{e_s(\mathrm{Ta})(1 - \mathrm{RH})}{0.000\,643p_s + \dfrac{\partial e_s}{\partial \mathrm{Ta}}},$$

$$e_s(\mathrm{Ta}) = 6.1078\exp\left(\frac{17.27\mathrm{Ta}}{\mathrm{Ta} + 237.3}\right),$$

$$P_c(\mathrm{Tw}) = \frac{1}{1 + \exp(\mathrm{Tw} - T_0)},$$

$$P_1(\mathrm{Tw}) = \frac{1}{1 + \exp\left(\dfrac{\mathrm{Tw} - T_0 + \Delta T}{\Delta S}\right)},$$

$$P_2(\mathrm{Tw}) = \frac{1}{1 + \exp\left(\dfrac{\mathrm{Tw} - T_0 - \Delta T}{\Delta S}\right)},$$

$$\Delta T = 0.215 - 0.099\,\mathrm{RH} + 1.018\,\mathrm{RH}^2,$$

$$\Delta S = 2.374 - 1.634\,\mathrm{RH},$$

$$T_0 = -5.87 - 0.1042\,Z + 0.0885\,Z^2 + 16.06\,\mathrm{RH} - 9.614\,\mathrm{RH}^2,$$

where Tw is the wet-bulb temperature, p_s is air pressure, Ta is air temperature, RH is relative humidity ranging from 0 to 1, and e_s is the saturated vapor pressure at Ta.

APPENDIX B

Pluvio Gauges Correction of Precipitation Measurements

Table B1 shows the wetting constants per case (mm 12 h^{-1}) for synoptic (synop) gauge and precipitation phase (Michelson 2004).

TABLE B2. Daily evaporation loss constants for synoptic gauge type (mm day^{-1}) (Michelson 2004).

Month	Evaporation constants
Jan	0.01
Feb	0.02
Mar	0.03
Apr	0.04
May	0.09
Jun	0.15
Jul	0.16
Aug	0.08
Sep	0.02
Oct	0.01
Nov	0.01
Dec	0.01

TABLE B3. Gauge constants [Eqs. (8) and (9)] for liquid and solid precipitation [mm $(12\,h)^{-1}$] (Michelson 2004).

Precip phase	Gauge constants
Liquid	0
Solid β_0	0.045 87
Solid β_1	0.236 77
Solid β_2	0.017 979
Solid β_3	−0.015 407

Table B2 lists daily evaporation loss constants for synoptic gauge type (mm day^{-1}) (Michelson 2004).

Table B3 displays the gauge constants [Eqs. (8) and (9)] for liquid and solid precipitation (mm $12\,h^{-1}$) (Michelson 2004).

REFERENCES

Abermann, J., M. Eckerstorfer, E. Malnes, and B. Hansen, 2019: A large wet snow avalanche cycle in west Greenland quantified using remote sensing and in situ observations. *Nat. Hazards*, **97**, 517–534, https://doi.org/10.1007/s11069-019-03655-8.

Allerup, P., H. Madsen, and F. Vejen, 1998: Estimating true precipitation in Arctic areas. *Proc. Nordic Hydrological Conf.*, Helsinki, Finland, Nordic Hydrological Programme Rep. 44, 1–9.

Bales, R. C., and Coauthors, 2009: Annual accumulation for Greenland updated using ice core data developed during 2000–2006 and analysis of daily coastal meteorological data. *J. Geophys. Res.*, **114**, D06116, https://doi.org/10.1029/2008JD011208.

Berghuijs, W. R., R. A. Woods, and M. Hrachowitz, 2014: A precipitation shift from snow towards rain leads to a decrease in streamflow. *Nat. Climate Change*, **4**, 583–586, https://doi.org/10.1038/nclimate2246.

Bogdanova, E. G., B. M. Ilyin, and I. V. Dragomilova, 2002: Application of a comprehensive bias-correction model to precipitation measured at Russian North Pole drifting stations. *J. Hydrometeor.*, **3**, 700–713, https://doi.org/10.1175/1525-7541(2002)003<0700:AOACBC>2.0.CO;2.

Box, J. E., and Coauthors, 2006: Greenland ice sheet surface mass balance variability (1988–2004) from calibrated Polar MM5 output. *J. Climate*, **19**, 2783–2800, https://doi.org/10.1175/JCLI3738.1.

Bromwich, D., R. Cullather, Q. Chen, and B. Csatho, 1998: Evaluation of recent precipitation studies for Greenland ice sheet. *J. Geophys. Res.*, **103**, 26 007–26 024, https://doi.org/10.1029/98JD02278.

Cappelen, J., Ed., 2013: Greenland DMI historical climate data collection 1873-2012—With Danish abstracts. DMI Rep. 13-04, 75 pp., https://www.dmi.dk/fileadmin/Rapporter/TR/tr13-04.pdf.

——, 2020: Weather observations from Greenland 1958-2019—Observation data with description. DMI Rep. 20-08, 33 pp., https://www.dmi.dk/fileadmin/user_upload/Rapporter/TR/2020/DMIRep20-08.pdf.

Chen, Q. S., D. H. Bromwich, and L. Bai, 1997: Precipitation over Greenland retrieved by a dynamic method and its relation to cyclonic activity. *J. Climate*, **10**, 839–870, https://doi.org/10.1175/1520-0442(1997)010<0839:POGRBA>2.0.CO;2.

Colgan, W., H. Rajaram, R. S. Anderson, K. Steffen, H. J. Zwally, T. Phillips, and W. Abdalati, 2011: The annual glaciohydrology cycle in the ablation zone of the Greenland ice sheet: Part 1. Hydrology model. *J. Glaciol.*, **57**, 697–709, https://doi.org/10.3189/002214311797409668.

Cullather, R., S. M. J. Nowicki, B. Zhao, and M. J. Suarez, 2014: Evaluation of the surface representation of the Greenland ice sheet in a general circulation model. *J. Climate*, **27**, 4835–4856, https://doi.org/10.1175/JCLI-D-13-00635.1.

Ding, B. H., K. Yang, J. Qin, L. Wang, Y. Y. Chen, and X. B. He, 2014: The dependence of precipitation types on surface elevation and meteorological conditions and its parameterization. *J. Hydrol.*, **513**, 154–163, https://doi.org/10.1016/j.jhydrol.2014.03.038.

Doyle, S. H., and Coauthors, 2015: Amplified melt and flow of the Greenland ice sheet driven by late-summer cyclonic rainfall. *Nat. Geosci.*, **8**, 647–653, https://doi.org/10.1038/ngeo2482.

ECMWF, 2008: Part IV: Physical processes. IFS Documentation CY33R1, 162 pp., https://www.ecmwf.int/en/elibrary/9227-ifs-documentation-cy33r1-part-iv-physical-processes.

Ettema, J., M. R. van den Broeke, E. van Meijgaard, W. J. van de Berg, J. L. Bamber, J. E. Box, and R. C. Bales, 2009: Higher surface mass balance of the Greenland ice sheet revealed by high resolution climate modeling. *Geophys. Res. Lett.*, **36**, L12501, https://doi.org/10.1029/2009GL038110.

Fettweis, X., and Coauthors, 2020: GrSMBMIP: Intercomparison of the modelled 1980–2012 surface mass balance over the Greenland ice sheet. *Cryosphere*, **14**, 3935–3958, https://doi.org/10.5194/tc-14-3935-2020.

Førland, E. J., and Coauthors, 1996: Manual for operational correction of Nordic precipitation data. DNMI-Klima Rep. 24/96, 66 pp., https://www.met.no/publikasjoner/met-report/met-report-1996/_/attachment/download/ea2cb006-688a-408f-a60c-9f6306843cc0:e16a138129a1d1896cff764ab3eb2cc42aefb160/MET-report-24-1996.pdf.

Goodison, B. E., P. Y. T. Louie, and D. Yang, 1998: WMO Solid Precipitation Measurement Intercomparison. Instruments and Observing Methods Rep. 67, WMO7TD-872, 318 pp., https://library.wmo.int/doc_num.php?explnum_id=9694.

Günther, T., and B. Graf, 1991: II: Wind related errors in different methods of solid precipitation measurement. *Hydrol. Processes*, **5**, 233–241, https://doi.org/10.1002/hyp.3360050303.

Hock, R., and B. Holmgren, 2005: A distributed surface energy balance model for complex topography and its application to Storglaciären, Sweden. *J. Glaciol.*, **51**, 25–36, https://doi.org/10.3189/172756505781829566.

Lewis, G., and Coauthors, 2019: Recent precipitation decrease across the western Greenland ice sheet percolation zone. *Cryosphere*, **13**, 2797–2815, https://doi.org/10.5194/tc-13-2797-2019.

Lindström, G., B. Johansson, M. Persson, M. Gardelin, and S. Bergström, 1997: Development and test of the distributed HBV-96 hydrological model. *J. Hydrol.*, **201**, 272–288, https://doi.org/10.1016/S0022-1694(97)00041-3.

Loth, B., H. F. Graf, and J. M. Oberhuber, 1993: Snow cover model for global climate simulations. *J. Geophys. Res.*, **98**, 10 451–10 464, https://doi.org/10.1029/93JD00324.

Mernild, S. H., E. Hanna, J. R. McConnell, A. P. Beckerman, J. C. Yde, J. K. Malmros, and K. Stefen, 2015: Greenland precipitation trends in a long-term instrumental climate context (1890–2012): Evaluation of coastal and ice core records. *Int. J. Climatol.*, **35**, 303–320, https://doi.org/10.1002/joc.3986.

Metcalfe, J. R., and B. E. Goodison, 1993: Correction of Canadian winter precipitation data. *Proc. Eighth Symp. on Meteorological Observations and Instrumentation*, Anaheim, CA, Amer. Meteor. Soc., 338–343.

——, S. Ishida, and B. E. Goodison, 1994: A corrected precipitation archive for the Northwest Territories of Canada. University of Saskatchewan, http://www.usask.ca/geography/MAGS/Data/Public_Data/precip_corr/pcpncor_e.htm.

Michelson, D. B., 2004: Systematic correction of precipitation gauge observations using analyzed meteorological variables. *J. Hydrol.*, **290**, 161–177, https://doi.org/10.1016/j.jhydrol.2003.10.005.

Milkovic, J., 1989: Preliminary results of the WMO field intercomparison in Yugoslavia. *Proc. Int. Workshop on Precipitation Measurement*, St. Moritz, Switzerland, ETH Zurich, 145–149.

——, 2002: Some results of the WMO intercomparison in Croatia. *Proc. WCRP Workshop on Determination of Solid Precipitation in Cold Climate Regions*. Fairbanks, AK, WCRP, 1–6.

Noël, B., W. J. van de Berg, E. van Meijgaard, P. Kuipers Munneke, R. S. W. Van de Wal, and M. R. Van den Broeke, 2015: Evaluation of the updated regional climate model RACMO2.3: Summer snowfall impact on the Greenland ice sheet. *Cryosphere*, **9**, 1831–1844, https://doi.org/10.5194/tc-9-1831-2015.

——, ——, ——, R. S. W. van de Wal, and M. R. van den Broeke, 2018: Modelling the climate and surface mass balance of polar ice sheets using RACMO2—Part 1: Greenland (1958–2016). *Cryosphere*, **12**, 811–831, https://doi.org/10.5194/tc-12-811-2018.

Ohmura, A., and N. Reeh, 1991: New precipitation and accumulation maps for Greenland. *J. Glaciol.*, **37**, 140–148, https://doi.org/10.1017/S0022143000042891.

Rubel, F., and M. Hantel, 1999: Correction of daily rain gauge measurements in the Baltic Sea drainage basin. *Nord. Hydrol.*, **30**, 191–208, https://doi.org/10.2166/nh.1999.0011.

Screen, J. A., and I. Simmonds, 2012: Declining summer snowfall in the Arctic: Causes, impacts and feedbacks. *Climate Dyn.*, **38**, 2243–2256, https://doi.org/10.1007/s00382-011-1105-2.

Sevruk, B., 1982: Method of correction for systematic error in point precipitation measurement for operational use. WMO Operational Hydrology Rep. 21, WM0-589, 91 pp., https://library.wmo.int/doc_num.php?explnum_id=1238.

——, and W. R. Hamon, 1984: International comparison of national precipitation gauges with a reference pit gauge. WMO Instrument and Observing Methods Rep. 17, 111 pp., https://library.wmo.int/doc_num.php?explnum_id=9533.

——, and S. Klemm, 1989: Types of standard precipitation gauges. *Proc. Int. Workshop on Precipitation Measurement*, St. Moritz, Switzerland, ETH Zurich, 227–236.

Smith, L. C., and Coauthors, 2015: Efficient meltwater drainage through supraglacial streams and rivers on the southwest Greenland ice sheet. *Proc. Natl. Acad. Sci. USA*, **112**, 1001–1006, https://doi.org/10.1073/pnas.1413024112.

Steffen, K., and J. E. Box, 2001: Surface climatology of the Greenland ice sheet: Greenland climate network 1995–1999. *J. Geophys. Res.*, **106**, 33 951–33 964, https://doi.org/10.1029/2001JD900161.

Steffensen, P., 1996: Standard normal homogeneity test for Windows. DMI Tech. Rep. 96-13, 35 pp.

——, F. L. Larsen, and J. Cappelen, 1993: Homogeneity test of climatological data. DMI Tech. Rep. 93-12, 22 pp., https://www.dmi.dk/fileadmin/Rapporter/TR/tr93-12.pdf.

Tompkins, A. M., K. Gierens, and G. Rädel, 2007: Ice supersaturation in the ECMWF integrated forecast system. *Quart. J. Roy. Meteor. Soc.*, **133**, 53–63, https://doi.org/10.1002/qj.14.

Van As, D., and Coauthors, 2017: The Programme for Monitoring of the Greenland Ice Sheet: PROMICE science report 2016. Geological Survey of Denmark and Greenland, 73 pp., http://promice.org/PromiceDataPortal/api/download/92acb911-e952-4128-9030-ce34ab284715/PROMICE_annual_report_2016.pdf.

Van den Broeke, M., and Coauthors, 2009: Partitioning recent Greenland mass loss. *Science*, **326**, 984–986, https://doi.org/10.1126/science.1178176.

Van Meijgaard, E., L. H. Van Ulft, W. J. Van de Berg, F. C. Bosveld, B. J. J. M. Van den Hurk, G. Lenderink, and A. P. Siebesma, 2008: The KNMI regional atmospheric climate model RACMO version 2.1. KNMI Tech. Rep. 302, 50 pp., https://cdn.knmi.nl/system/data_center_publications/files/000/068/251/original/tr302_racmo2v1.pdf?1495621093.

Van Wessem, J. M., C. H. Reijmer, J. T. M. Lenaerts, W. J. Van de Berg, M. R. Van den Broeke, and E. Van Meijgaard, 2014: Updated cloud physics in a regional atmospheric climate model improves the modelled surface energy balance of Antarctica. *Cryosphere*, **8**, 125–135, https://doi.org/10.5194/tc-8-125-2014.

Walsh, J. E., V. Kattsov, D. Portis, and V. Meleshko, 1998: Arctic precipitation and evaporation: Model results and observational estimates. *J. Climate*, **11**, 72–87, https://doi.org/10.1175/1520-0442(1998)011<0072:APAEMR>2.0.CO;2.

WMO, 1993: Final report of the sixth session. International Organizing Committee for the WMO Solid Precipitation Measurement Intercomparison, WMO Rep., 140 pp., https://library.wmo.int/doc_num.php?explnum_id=6332.

——, 2008: Guide to meteorological instruments and methods of observation. WMO-881, 681 pp.

Yamazaki, T., 2001: A one-dimensional land surface model adaptable to intensely cold regions and its applications in eastern Siberia. *J. Meteor. Soc. Japan*, **79**, 1107–1118, https://doi.org/10.2151/jmsj.79.1107.

Yang, D., and Coauthors, 1995: Accuracy of Tretyakov precipitation gauge: Results of WMO intercomparison. *Hydrol. Processes*, **9**, 877–895, https://doi.org/10.1002/hyp.3360090805.

——, B. E. Goodison, C. B. Benson, and S. Ishida, 1998: Adjustment of daily precipitation data at 10 climate stations in Alaska: Application of World Meteorological Organization intercomparison results. *Water Resour. Res.*, **34**, 241–256, https://doi.org/10.1029/97WR02681.

——, S. Ishida, B. E. Goodison, and T. Gunther, 1999: Bias correction of daily precipitation measurements for Greenland. *J. Geophys. Res.*, **104**, 6171–6181, https://doi.org/10.1029/1998JD200110.

——, K. Kane, and Z. Zhang, 2005: Bias correction of long-term (1973–2004) daily precipitation data over the northern regions. *Geophys. Res. Lett.*, **32**, 19 501–19 506, https://doi.org/10.1029/2005GL024057.

Yang, Z.-L., R. E. Dickinson, A. Robock, and K. Y. Vinnikov, 1997: Validation of the snow submodel of the Biosphere–Atmosphere Transfer Scheme with Russian snow cover and meteorological observational data. *J. Climate*, **10**, 353–373, https://doi.org/10.1175/1520-0442(1997)010<0353:VOTSSO>2.0.CO;2.